catalysts

MDPI

Article

Effects of Sodium-to-OSDA Ratio in the Synthesis Gel on SSZ-39 Formation and Material Properties

Zheng Cui [1], Charles E. Umhey [2], Daniel F. Shantz [1,*] and Jean-Sabin McEwen [2,3,4,5,6,*]

[1] Department of Chemical and Biomolecular Engineering, Tulane University, 6823 St. Charles Avenue, New Orleans, LA 70118, USA; zcui@tulane.edu
[2] The Gene and Linda Voiland School of Chemical Engineering and Bioengineering, Washington State University, Pullman, WA 99164, USA; charles.umhey@wsu.edu
[3] Institute for Integrated Catalysis, Pacific Northwest National Laboratory, Richland, WA 99352, USA
[4] Department of Physics and Astronomy, Washington State University, Pullman, WA 99164, USA
[5] Department of Chemistry, Washington State University, Pullman, WA 99164, USA
[6] Department of Biological Systems Engineering, Washington State University, Pullman, WA 99164, USA
* Correspondence: dshantz@tulane.edu (D.F.S.); js.mcewen@wsu.edu (J.-S.M.)

Abstract

This work quantifies how varying the Na/OSDA ratio in the synthesis gel (at fixed total [OH] content) affects the formation of SSZ-39, its growth kinetics, and the composition of the products obtained. It was found that it is possible to make phase-pure SSZ-39 with Si/Al ratios varying from 6.3 to 10.7 with Na/OSDA ratios from 9.1 to 1.7 in the synthesis gel. Higher Na/OSDA ratios lead to faster crystallization, supporting the hypothesis that FAU dissolution is the rate-limiting step in SSZ-39 synthesis when FAU serves as the aluminum source. DFT modeling suggests that, in the presence of OSDA molecules, increased Na content lowers the energy penalty for placing Al atoms in close proximity, which may explain why higher NaOH/OSDA ratios experimentally yield lower Si:Al ratios. This work offers another way to control the framework composition and potentially impact the local structure of the SSZ-39 that is obtained. Cobalt titration was performed to probe the presence of so-called aluminum pairs in samples made with different Na/OSDA ratios. The cobalt uptake in the H-form products is consistently low and suggests that factors other than aluminum pairing, such as solution pH, could be important in influencing the cobalt uptake.

Keywords: SSZ-39; zeolite growth; small-pore zeolites

check for updates

Academic Editor: Narendra Kumar

Received: 10 September 2025
Revised: 11 October 2025
Accepted: 13 October 2025
Published: 16 October 2025

Citation: Cui, Z.; Umhey, C.E.; Shantz, D.F.; McEwen, J.-S. Effects of Sodium-to-OSDA Ratio in the Synthesis Gel on SSZ-39 Formation and Material Properties. *Catalysts* **2025**, *15*, 989. https://doi.org/10.3390/catal15100989

Copyright: © 2025 by the authors. Licensee MDPI, Basel, Switzerland. This article is an open access article distributed under the terms and conditions of the Creative Commons Attribution (CC BY) license (https://creativecommons.org/licenses/by/4.0/).

1. Introduction

Despite their technological significance, a molecular description of how zeolites nucleate and grow has eluded the community [1–6]. As a result, many properties of interest such as framework composition, local ordering of heteroatoms, crystal size, etc., cannot be controlled rationally, but rather using a trial-and-error approach [7–12]. Being able to control properties more directly through synthesis would lead to more active and selective catalysts, with immediate benefits for zeolites used in the chemical and petrochemical industry.

One aspect of this space that has long attracted attention in the zeolite community is the formation of so called "aluminum pairs" within the zeolite framework. The basic idea is that the presence of two aluminum atoms close to one another in the framework can stabilize extra-framework species that have desirable catalytic properties. Going back to work from Iglesia and Rimer's lab in the 1990s on aluminum pairs stabilizing metal

centers [13], as well as the seminal UV-Vis studies by the Wichterlova and coworkers [14–18], these efforts have sought to clearly show the presence (and importance) of such aluminum centers. This has been and continues to be a vibrant area of research [19–30]. It is an intellectually interesting and technically important aspect in zeolite catalysis.

A recent series of papers from the Gounder and coworkers' lab has reported an interesting set of studies on SSZ-13 samples that were made with varying ratios of sodium and organic structure directing agent (OSDA) in the synthesis gel [7,31–34]. These materials appear to have different local arrangements of aluminum based on both cobalt titration and catalytic testing [35–37]. This intriguing finding motivates our current work.

In the current work, we report a study of the synthesis and characterization of zeolite SSZ-39 wherein we take a standard literature preparation and vary the sodium and OSDA content in the gel. SSZ-39 is the aluminosilicate analog of the AEI topology (ALPO4-18), [10,38–41] and is a small-pore zeolite that has shown potential applications in the selective catalytic reduction of NO and other applications [42–45]. Our lab has previously made and reported studies on SSZ-39, [46,47] a zeolite with a cage-like topology and the same building units as SSZ-13, but with differently shaped cages. Our reports show that samples of SSZ-13 and SSZ-39 with similar framework compositions and extra-framework copper contents display different catalytic properties [48]. There are several possible explanations for these findings; one could be the local arrangement of aluminum in the lattice. Here we explore this issue in SSZ-39, namely, whether it is possible to influence the composition and local aluminum arrangement of SSZ-39.

2. Results

2.1. Phase Selectivity as a Function of Gel Composition

The starting point was exploring the feasibility of making SSZ-39 modifying the standard synthesis used previously by varying the relative amount of sodium and the organic structure-directing agent (OSDA) *N*,*N*-dimethyl-3,5-dimethylpiperidinium hydroxide, where the two are in the ratio of 0.57:0.14 Na:OSDA. The total hydroxide content was kept fixed, so it was determined that Na + OSDA = 0.71 per the standard preparation. Table 1 summarizes the main findings of the synthesis work mapping out synthesis phase selectivity of SSZ-39.

Table 1. Summary of initial syntheses exploring feasibility of making SSZ-39 at different Na/OSDA values. Ratio of the standard preparation is in bold.

NaOH/OSDA	Ratio Value	Phase-Pure SSZ-39
0.68/0.03	22.6	No
0.66/0.05	13.2	No
0.64/0.07	9.14	Yes
0.60/0.11	5.45	Yes
0.57/0.14	**4.07**	**Yes**
0.51/0.2	2.55	Yes
0.45/0.26	1.73	Yes
0.42/0.29	1.45	No
0.39/0.32	1.22	No
0.33/0.38	0.87	No
0.21/0.5	0.42	No

The results in Table 1 show that it is possible to make phase-pure SSZ-39 with a NaOH/OSDA ratio of 9.1 to 1.7. It was decided to keep the total hydroxide content fixed, given that the pH is the most sensitive parameter in zeolite syntheses.

2.2. Effect of NaOH/ROH on Crystallization Kinetics and Framework Composition of SSZ-39

Given the possibility to form SSZ-39 over a wide range of NaOH/OSDA ratios, it was decided to investigate the crystallization kinetics of the most sodium-rich and most OSDA-rich gels that led to the formation of phase-pure SSZ-39. The relative fraction of FAU and AEI were estimated using powder X-ray diffraction of the intermediate solids.

The clearest conclusion from Figure 1 is that increasing the NaOH/OSDA of the gel leads to an increase in the crystallization kinetics. One possible explanation for this could be that with increased sodium content, the dissolution of the FAU is enhanced, which we postulated in prior work was the rate limiting step of SSZ-39 formation [46]. As shown in prior work, no broad feature in the 20–30 degree range of the PXRD pattern, supporting the absence of appreciable amorphous material [46]. This is consistent with our hypothesis that SSZ-39 forms rapidly after FAU dissolution. An interesting observation is that in the syntheses where phase-pure SSZ-39 was not formed, we observed two other outcomes. One was the formation of some SSZ-39 but the incomplete consumption of FAU. The second was the observation of FAU plus amorphous solids with no SSZ-39 present. It is somewhat surprising that no other zeolitic phases were observed by PXRD when SSZ-39 does not form.

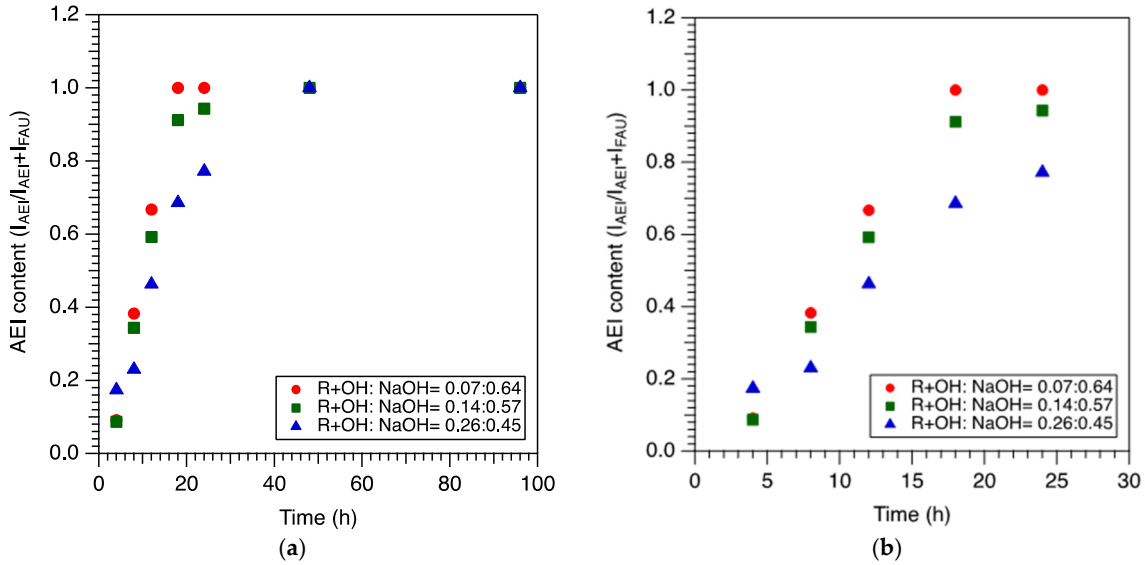


Figure 1. (**a**) Crystallization kinetics of three different SSZ-39 synthesis gels with 20% trans OSDA for the entire synthesis timeframe. (**b**) Crystallization kinetics of each synthesis gel for the first 30 h. Note: the 0.14:0.57 ratio is the standard preparation.

Figure 2 shows the TGA results for the fully crystallized samples at the 'standard' synthesis composition and the synthesis with the most OSDA or most NaOH that resulted in a phase-pure synthesis. There is a systematic trend in mass of OSDA lost, namely as the NaOH/OSDA of the gel increases, the weight loss decreases.

This indicates there is a modest enhancement of the amount of OSDA occluded in the as-synthesized zeolite with increasing OSDA content in the gel. Interestingly, compositional analysis of the samples shows the Si/Al ratio decreases as the NaOH/OSDA ratio in the gel increases, as summarized in Figure 3. Thus, decreasing the sodium content of the gel has the same effect as increasing the trans isomer content at a given OSDA content from a compositional viewpoint. Finally, it is noteworthy that the most sodium-rich gel that led to phase-pure SSZ-39 has a product Si/Al of 6.4. This was not a framework composition where one could access phase-pure SSZ-39 in prior work, as impurities of analcime or gismondine were typically observed [46,49].

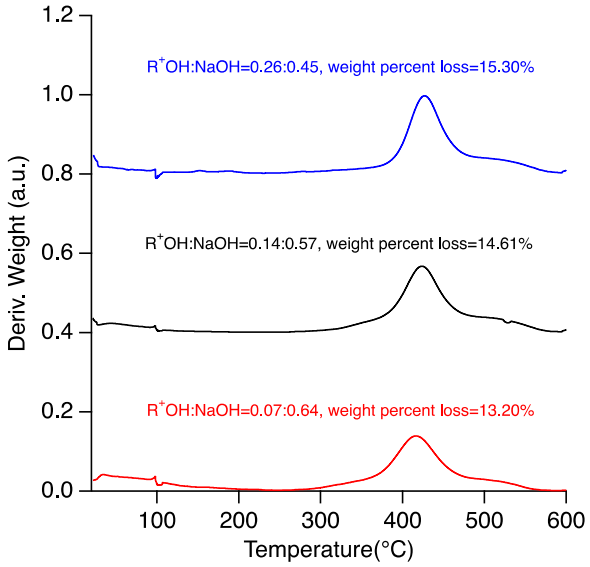


Figure 2. TGA results for the samples crystallized from the synthesis gels shown in Table 1.

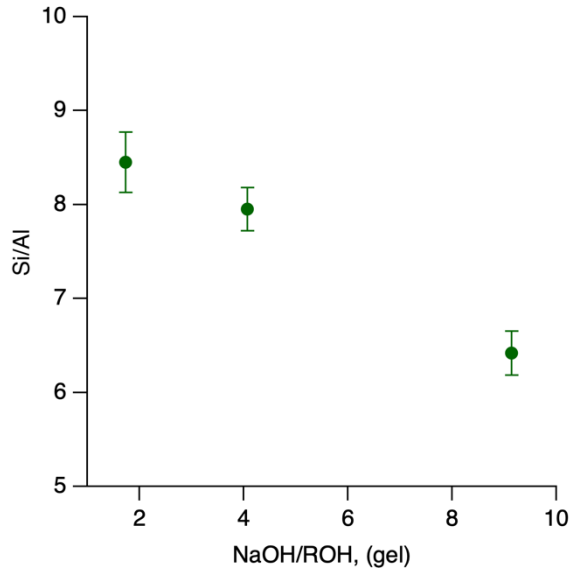


Figure 3. Si/Al of the products as a function of the NaOH/OSDA ratio.

These materials, consistent with our standard preparation led to cuboidal particles, which are typically 300–500 nm in size (Figure 4). This is consistent with the standard preparation and appears to indicate the NaOH/ROH ratio does not significantly impact SSZ-39 crystal morphology.

TGA measurements were performed to analyze the organic weight loss as a function of synthesis time. This is shown in Figure 5 in a plot of the derivative weight loss versus temperature. There are two notable features in this data. First is the weight loss at approximately 300 °C observed at synthesis times before full crystallization. This weight loss is attributed to OSDA that is adsorbed on or in the FAU early in the synthesis. The derivative weight loss for FAU incubated with 100 mM OSDA for 24 h shown as the bottom trace in each plot supports this claim. The second feature appears at approximately 430 °C, first noticeable at 8 h for both samples, which increases in intensity and shifts to approximately 10 degrees lower as the synthesis becomes complete. This feature is assigned to an OSDA in the SSZ-39 cages. As can be seen in Figure 5, the attenuation of the feature at 300 °C

occurs at shorter synthesis times. The TGA results appear consistent with XRD and SEM, confirming that there are significant amounts of SSZ-39 formed by 8–12 h of synthesis.

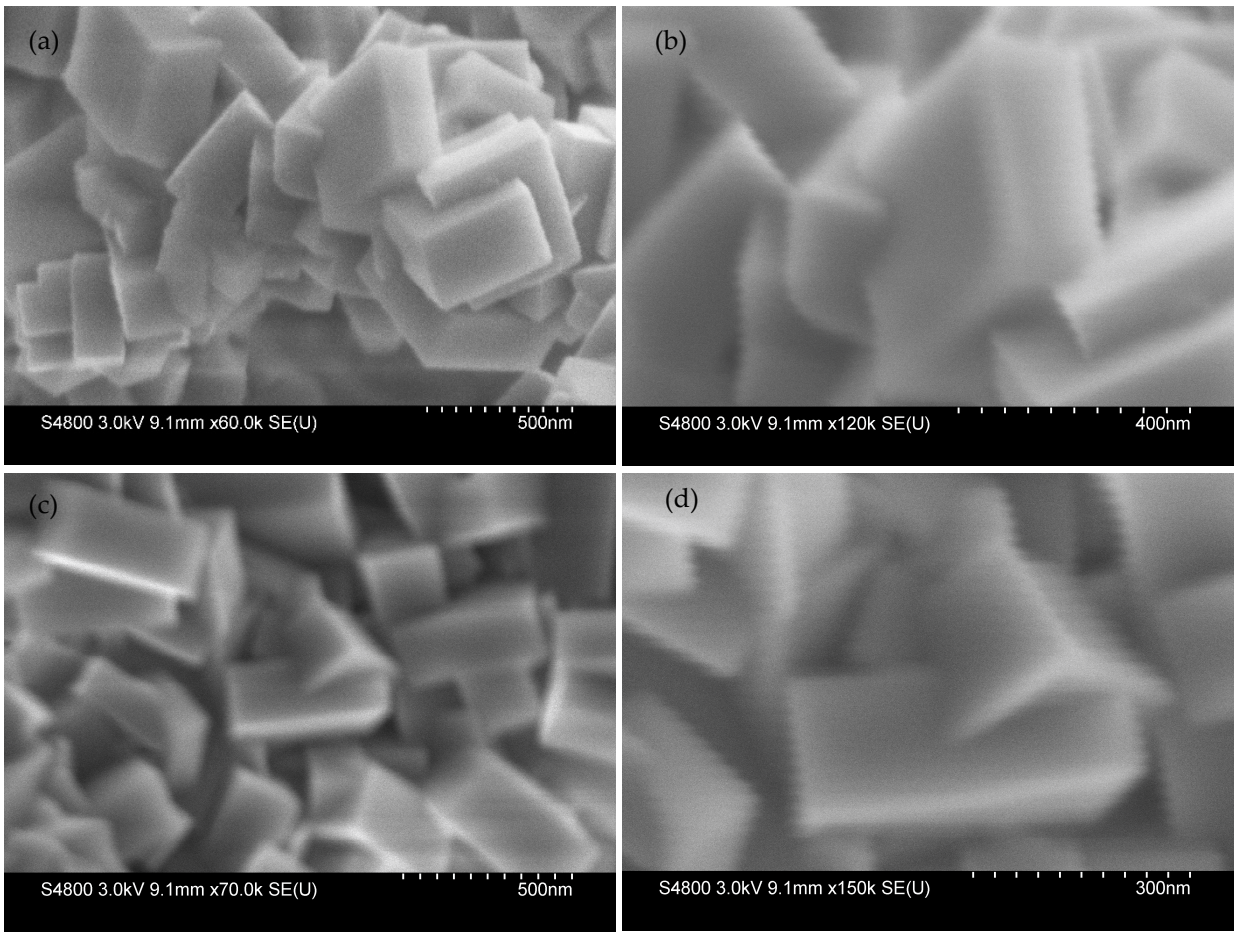


Figure 4. SEM images of samples made at an NaOH/OSDA ratio of 9.1 (**a**,**b**) and 1.7 (**c**,**d**).

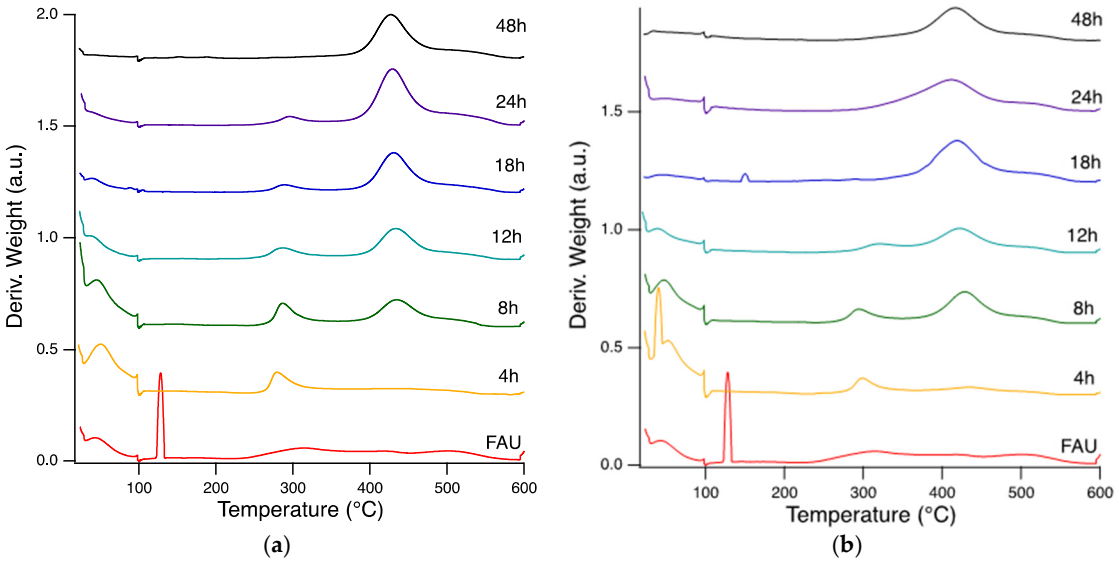


Figure 5. TGA results for the solids obtained from gels with (**a**) NaOH/OSDA of 1.73 and (**b**) NaOH/OSDA of 9.1.

The effect of sodium content on Si/Al ratios was probed using DFT calculations to evaluate how increasing the separation between Al atoms changed the ground state

energy of SSZ-39 systems when Al atoms were charge-compensated by Na cations. These calculations took place in a two-step process. First, the most favorable binding site for a single Na cation was determined by optimizing the geometry of SSZ-39 with a single Al atom and a Na cation. Each unique T site in SSZ-39 was considered as a potential Al site, and for each Al site each connected six and eight membered ring was tested as a potential binding site for Na. The most favorable site identified by this process was used as a starting point for the second step where each T site in the unit cell not violating Löwenstein's rule was tested as a possible site for a second Al atom charge compensated by a second sodium atom. The binding sites for the second Na cation were tested using the same procedure as for the first Na cation. Once each configuration had been optimized, relative energies were determined by subtracting the energy of the most favorable configuration from the energy of each configuration. As can be seen in Figure 6, these calculations show that increasing the number of Si atoms separating Al atoms from one to three only increases the average relative energy by 0.06 eV. Example conformations for different numbers separating Si atoms are shown in Figure 6. These results suggest that Al-Al separation has little impact on thermodynamic favorability in SSZ-39 when only sodium atoms act as a charge compensating species. Interestingly, a different trend emerges when OSDA molecules are present. Using data collected in our previous study on OSDA binding and Al distribution in SSZ-39 [37], average relative energies were computed for systems with exclusively OSDA molecules and a mixture of OSDA molecules and Na atoms. Increasing the number of Si atoms separating Al atoms from one to three results in a decrease in energy of 0.26 eV for systems with cis OSDAs, 0.15 eV for systems with a mixture of cis and trans OSDAs, and by 0.30 eV for systems with exclusively trans OSDAs. For systems containing exclusively cis or exclusively trans OSDAs, the most favorable separation is three Si atoms, while a mixture of cis and trans OSDAs has a slight preference (0.06 eV) for systems with a separation of two Si atoms compared to systems with a separation of three Si atoms. In systems with a mixture of OSDA molecules and Na cations the ideal separation is two Si atoms between each Al atom. In systems with cis OSDAs and Na cations increasing the separation of Al atoms from one Si atom to two decreases the energy by an average of 0.12 eV, while in systems with trans OSDAs and Na cations, a reduction of 0.13 eV is obtained. Unlike systems with exclusively Na, when OSDA molecules are present the thermodynamic favorability of Al pairs in SSZ-39 is sensitive to the Al-Al distance with pairs only separated by a single Si atom being unfavorable. These results, summarized in Figure 6, indicate that increasing the Na content in SSZ-39 decreases the energy penalty associated with placing Al atoms near each other, which may explain why a higher NaOH/OSDA ratio leads to a lower the Si:Al ratio. One potential reason for why OSDA molecules inhibit Al pairs with only a single Si atom separating the Al is steric effects caused by OSDAs being forced in close proximity to each other in order to charge-compensate nearby Al atoms.

The results above show that increasing the sodium content relative to the OSDA increases the crystallization kinetics and lowers the product Si/Al. Prior work from our lab has shown that increasing the trans content accelerated the crystallization kinetics and increased the Si/Al. This led us to combine these two aspects to estimate over how wide of a framework composition range one could make SSZ-39. Using a gel with a NaOH/ROH of 9.1 with a trans content of 14% led to a product with an Si/Al = 6.3 +/− 0.13. By contrast, using a gel with a NaOH/ROH of 1.7 with a trans content of 80% led to a product with an Si/Al = 10.7 +/− 0.15. This is a reasonably broad range, which has potential for tuning acid site density and potentially reactivity, metal siting, etc. It should also be noted the most silicon-rich material has a Si/Al slightly less than 11, implying that on average, each double six-membered ring in the SSZ-39 framework has one aluminum atom in it.

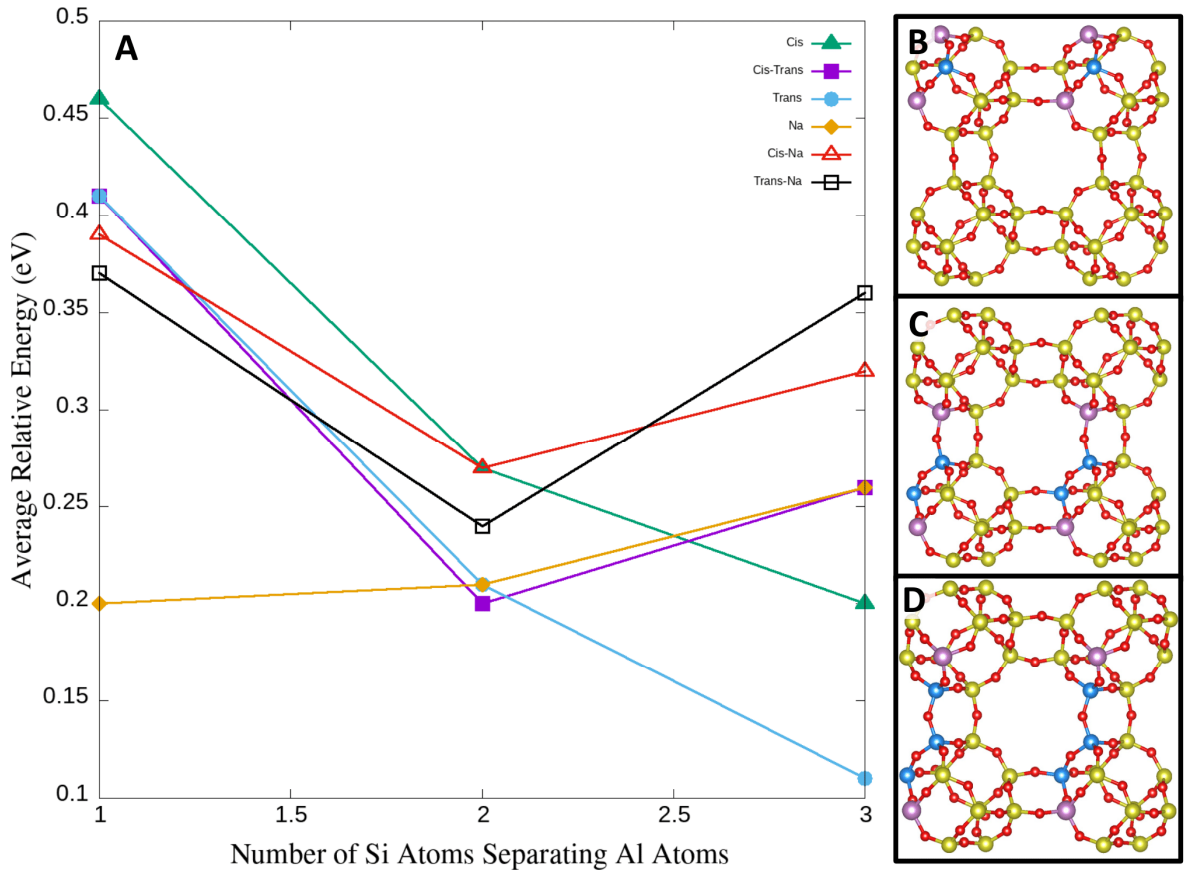


Figure 6. (**A**) Average relative energies for Al pair distributions in SSZ-39 as a function of the number of Si atoms separating each Al atom. (**B**–**D**) Examples of SSZ-39 with Al pairs separated by 1 (**B**), 2 (**C**), or 3 (**D**) Si atoms. For illustrative purposes, a subset of Si atoms along the shortest path between each Al pair is highlighted in blue. All other Si atoms are shown in yellow, while O and Al atoms are depicted in red and purple, respectively.

2.3. OSDA Binding Studies

NMR was used to monitor OSDA binding on FAU in the presence of sodium, to see if inhibition effects exist. The amount of OSDA adsorbed on FAU OSDA (and its isomers) was estimated by performing NMR on the liquid obtained after 24 h of incubating a mixture of 50 mM or 100 mM OSDA and varying concentrations of NaCl solution with FAU. The variability of the NMR results is +/− 0.047 (tube insertion, spectra acquisition, and profiling). Figure 7 shows the amount of OSDA adsorbed per gram of FAU by varying the concentration of NaCl. It is noted that less OSDA adsorbed on FAU as one increases with increasing the salt concentration based on the results of FAU incubation in 100 mM OSDA solution. The trans isomer is preferentially absorbed on FAU in the presence of NaCl as well (Figure 7), consistent with prior work from our lab [50].

Based on Figure 7, both the trans and cis isomers adsorb less on FAU in the presence of Na. This observation is not surprising, as it can be attributed to the phenomenon of competitive adsorption, in which multiple species within the system vie for a limited number of adsorption sites. This could explain the results of prior work that lower Na/Al ratio products are obtained when increasing the trans content of OSDA using in the synthesis.

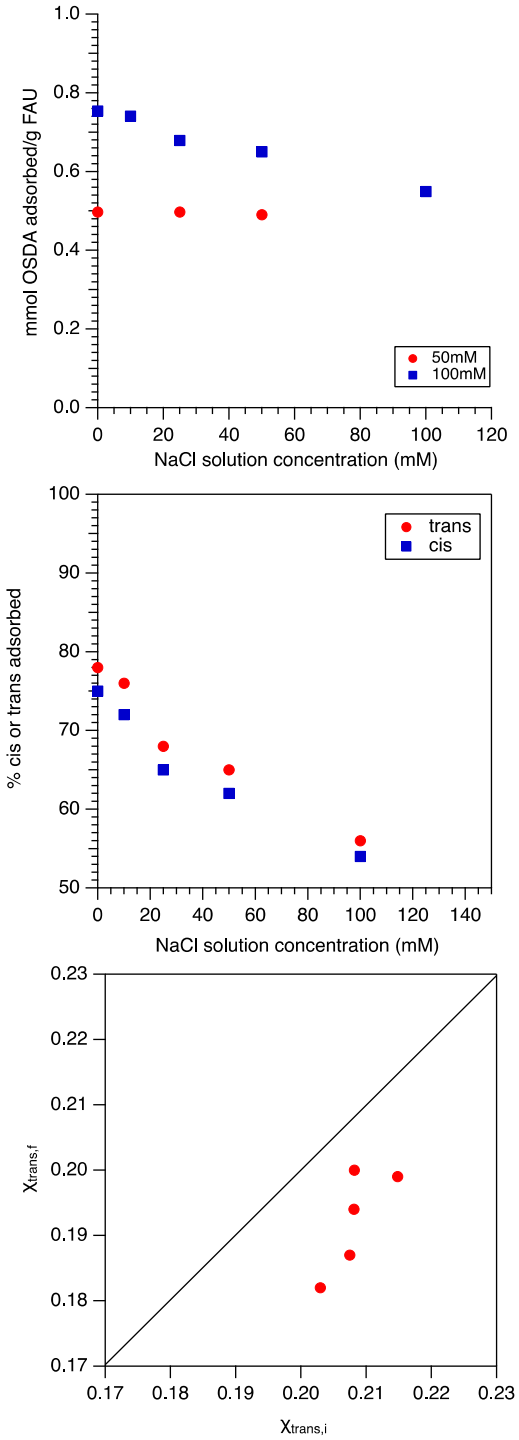


Figure 7. (**Top**) The amount of OSDA adsorbed to one gram of FAU after incubation by varying the concentration of NaCl solution. (**Middle**) Plot of trans isomer mole fraction in solution before (x-axis) and after (y-axis) incubation with FAU. (**Bottom**) Plot of percentage of cis/trans isomer adsorbed after incubation in 100 mM OSDA solution as a function of NaCl solution concentration.

Recently we published work comparing the binding energies of sodium and OSDA molecules in FAU and SSZ-39 using DFT calculations [50]. Na was found to have a binding energy of −289 kJ/mol in FAU and −302 kJ/mol in SSZ-39. Both Na conformations are shown in Figure S1. This binding energy is significantly less favorable than both the trans OSDA, which has binding energies of −364 kJ/mol and −462 kJ/mol in FAU and SSZ-39, respectively, and the cis OSDA, which were found to have binding energies of −358 kJ/mol and 460 kJ/mol in FAU and SSZ-39. The OSDA conformations can be seen in Figure S2

for the Cis OSDAs and Figure S3 for the trans OSDAs. These results predict that during competitive absorption, OSDA binding will be preferential to sodium binding, as shown in Figure 7, where a change in the concentration of NaOH from 0 mM to 100 mM only results in about a 20% decrease in the percentage of OSDA adsorbed in the zeolite framework. Moreover, this finding is consistent with an increased Na/OSDA ratio leading to increased crystallization kinetics. This is also consistent with increasing Na content enhancing the dissolution of the FAU, which we hypothesized in prior work was the rate-limiting step of SSZ-39.

2.4. Local Ordering of Aluminum

The results above show that it is possible to not only enhance the growth rate of SSZ-39 by increasing the NaOH/OSDA ratio in the gel, but it is also possible to decrease the Si/Al by doing the same. One motivation for this was the work from the Gounder lab reporting that is possible to vary the local aluminum ordering in SSZ-13 by varying the NaOH/OSDA ratio of the gel. This work shows a systematic change in the bulk composition. Cobalt titration was performed to explore this further. Figure 8 shows the Co/Al ratio of the three samples. Surprisingly, there is very low cobalt uptake and no obvious change in the cobalt uptake over the three zeolites studied. This is surprising given the range of Si/Al of these materials, as one would expect more aluminum pairs to be present as the Si/Al decreases. More recent work from our lab has suggested that the cobalt exchange is highly sensitive to the solution pH [50]. Ongoing work is investigating the source of this phenomenon and aims to more broadly understand whether factors beyond the amount of aluminum pairs in the zeolite influence cobalt exchange; results will be reported elsewhere.

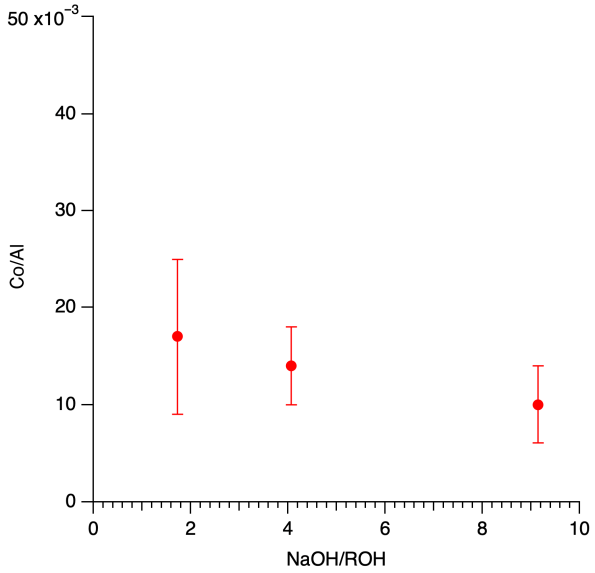


Figure 8. Co/Al ratio of the samples (H-form) with different NaOH/OSDA ratio in synthesis gel.

3. Discussion

The results demonstrate that synthesizing phase-pure SSZ-39 is feasible over a wide range of Na/OSDA ratios, ranging from 9.1 to 1.7. Moreover, increasing sodium content enhances crystallization kinetics. This observation is consistent with sodium playing a pivotal role in the dissolution of FAU, which prior work indicates is a key step in SSZ-39 formation. As the OSDA content in the gel increases, there is a small increase in the amount of OSDA occluded in the as-synthesized zeolite, as indicated by TGA results. Additionally, as the Na/OSDA ratio decreases, the Si/Al ratio in the zeolite samples correspondingly increases, which is consistent with our DFT-based model. By varying the Na/OSDA ratio

and the trans content of OSDA used in synthesis, samples were formed within a Si/Al range of 6.3–10.7, offering potential to fine-tune acid site density and reactivity. A liquid-phase adsorption study revealed that the amount of OSDA adsorbed on FAU declines when salt concentration rises, with the trans isomer displays an adsorption preference. This performance can be attributed to competitive adsorption or electrostatic screening, aligning with prior arguments that higher sodium content bolsters FAU dissolution, accelerating SSZ-39 formation kinetics. DFT results show that OSDA molecules bind more strongly to FAU and SSZ-39 than sodium, potentially explaining the observed preferential uptake of OSDA molecules over sodium atoms. Cobalt titration results are surprising, indicating a low cobalt (<0.03 Co/Al) uptake over all samples. This is being explored further and will be reported elsewhere.

4. Materials and Methods

4.1. Materials

Ludox HS-40 colloidal silica (40 wt.% suspension in H_2O) was purchased from Sigma-Aldrich. Faujasite (FAU) (SiO_2:Al_2O_3 = 5.2:1) was obtained from Zeolyst (Conshohocken, PA). Sodium hydroxide pellets (ACS grade) and 3-(trimethyisilyl) propionic-2,2,3,3-d4 acid, sodium salt (98 atom % D) were purchased from Sigma Aldrich (St. Louis, MO, USA). N, N-Dimethyl-3,5-dimethylpiperidinium hydroxide (35 wt%, with trans isomer content of 20%) was purchased from SACHEM (Austin, TX, USA). Cobalt (II) nitrate hexahydrate (99%) and deuterium oxide (99.8 atom % D) were purchased from Thermo Scientific Chemicals (Waltham, MA, USA). All reagents were used as received.

4.2. SSZ-39 Synthesis

The SSZ-39 synthesis was based on prior work in our lab and prior reports by Dusselier and coworkers [49]. SSZ-39 was synthesized using FAU (SiO_2:Al_2O_3 = 5.2:1) as the aluminum source from a gel composition of 1 SiO_2: 0.033 Al: x NaOH: y R^+OH^-: 28 H_2O (Si/Al = 30), where x + y = 0.71 in all cases (standard preparation, x = 0.57, y = 0.14). As an example, SSZ-39 was synthesized as follows. First, 0.57 g of NaOH was weighed out and dissolved in 9.46 g of DI water, followed by adding 3.41 g of Ludox HS-40 colloidal silica. Then, 1.59 g of 35 wt.% organic structure-directing agent (OSDA) solution (mixer of trans and cis isomer, 20% trans by NMR) was added to this solution. To this mixture, 0.17 g of FAU was added and mixed for 2 h at room temperature while stirring on a stir plate. The mixture was then transferred to two Teflon-lined autoclaves and heated at 140 °C while rotating at 60 rpm for the indicated time ranging from 4 to 96 h. The samples were then cooled down for 2 h, followed by filtration, washing with DI water until the filtrate pH was approximately 7, and dried at 100 °C overnight.

4.3. OSDA Adsorption Studies

OSDA solutions ranging in concentration from 50 mM to 250 mM were prepared from 35 wt%, 20% trans content OSDA obtained from SACHEM (Austin, TX, USA). The OSDA concentrations were determined by NMR using TMSP as an internal chemical shift reference and quantitative standard (300 µL of a 10 mM TMSP solution). One gram of FAU was added to 10 mL of OSDA solution, which was then stirred for 24 h at room temperature. Spectra were acquired with a 20 s delay time and 128 scans. Centrifugation at 5000 rpm for 20 min was performed to separate the liquid from the solids. A total of 300 µL of this solution was pipetted out and added to the same amount of 10 mM TMSP solution in the NMR tube, and NMR was performed the same way as before adsorption.

4.4. Cobalt Titration

Cobalt titration was performed using the method described by Di Iorio et al. [7] NH_4-SSZ-39 was prepared via aqueous phase ion-exchange. An amount of 0.18 g of calcined sample was exchanged in 27 mL of 1.0 M NH_4NO_3 solution at room temperature for 24 h (150 mL/g solids), followed by washing with 300 mL DI water. The sample was then dried at 100 °C overnight. It was then converted to H-SSZ-39 by calcination at 550 °C. The cobalt exchange was performed by adding 0.15 g of calcined sample to 24 mL of 0.25 M $Co(II)(NO_3)_2$ solution (150 mL/g sample). This solution was stirred at room temperature for 4 h, then filtered and washed with 10 mL of deionized water four times and dried at 100 °C overnight after the first exchange. The sample was calcined at 550 °C before being exchanged again with a 0.5 M $Co(II)(NO_3)_2$ solution (150 mL/g sample). The filtration and calcination were performed the same way as after the first exchange before EDS analysis.

4.5. Analytical

Powder X-ray diffraction patterns were measured using a Rigaku (Woodlands, TX, USA) Benchtop MiniFlex 600 X-ray diffractometer with Cu-Kα (l = 1.5418 Å) radiation operating at 40 kV and 15 mA. Diffraction patterns were measured in the range of 4−50° 2θ with a scanning speed of 1°/min. Field-emission scanning electron microscopy (FE-SEM) was carried out using a Hitachi (Tokyo, Japan) 4800 high-resolution scanning electron microscope operating at 3 kV. Energy-dispersive X-ray spectroscopy (EDS) was performed using a Hitachi (Tokyo, Japan) S3400 system (30 V, 100 mA) for elemental analysis of the catalyst samples. Nitrogen adsorption measurements were performed using a Micromeritics (Norcross, GA, USA) ASAP 2020 system at 77 K. Approximately 0.05 g of calcined sample was degassed at 573 K for 18 h under high vacuum prior to each analysis. Micropore volumes were determined based on the volume of nitrogen adsorbed at a $p/p_o = 0.1$, and external surface areas were calculated by the alpha-s method. Thermal gravimetric analyses (TGA) were performed using a TA instruments (New Castle, DE) Q500 over a temperature range of 25–700 °C and a temperature ramping rate of 5 °C/min under flowing air. All ^{1}H NMR spectra were performed on a Bruker (Billerica, MA, USA) DRX 500 MHz NMR at room temperature. An inverse BBI probe was used. The resonance frequency of ^{1}H was 500.13 MHz, and the presaturation pulse sequence for water suppression was used to acquire ^{1}H NMR spectra. ^{1}H NMR spectra of the filtrate recovered from the time series experiment were obtained from single pulse acquisition with a 30° pulse angle. Spectra were acquired with a 5 s delay time and 64 scans. For the ^{1}H NMR of the OSDA binding study, TMSP was used as an internal chemical shift reference as well as a quantitative standard (300 µL of a 10 mM solution). Spectra were acquired with a 20 s delay time, and 128 scans were accumulated. For the analysis of the XRD shown, to estimate the relative amount of FAU and AEI, we use the integrated peak intensity of the FAU peak at 6.12° 2θ and the AEI peak 9.5° 2θ, i.e., the fraction of AEI is equal to $I_{AEI,9.5}/(I_{AEI,9.5} + I_{FAU,6.12})$. In prior work, we used the peak heights instead of integrated intensities; we believe using the peak areas is more robust.

4.6. DFT Calculations

Density functional theory calculations were performed using the Vienna Ab initio Simulation Package (VASP) version 6 [51–54]. The interactions between valence and core electrons were modeled using the projector augmented wave method, [55] using PAW potentials released by VASP developers in 2017. The optB86b-vdW exchange correlation functional was used for all VASP calculations [56]. A 1 × 1 × 1 KPOINT mesh was used to sample the Brillouin zone for FAU while a 2 × 2 × 1 KPOINT mesh was used for SSZ-39. In both cases Gaussian smearing was used with a width of 0.2 eV. Self-consistent field cycles

were considered converged once the total energy difference between steps was less than 1×10^{-5} eV. The optimized unit cell of SSZ-39 [37] and FAU [50] were the same as those that were given in our previous work. Geometries were considered converged when the norms of all forces were smaller than 0.02 eV/Å.

Supplementary Materials: The following supporting information can be downloaded at https://www.mdpi.com/article/10.3390/catal15100989/s1, Figure S1: Most favorable Na binding positions in FAU and SSZ-39, Figure S2: Most favorable cis OSDA binding positions in FAU and SSZ-39, and Figure S3: Most favorable trans OSDA binding positions in FAU and SSZ-39. Sodium_Paper_SI_Catalysts.pdf; Cif files: for each geometry tested in this paper are available in the folder Cif_Files.zip. Naming conventions for the Cif files are described in the SI.

Author Contributions: Conceptualization, D.F.S. and Z.C.; methodology D.F.S., Z.C., C.E.U. and J.-S.M.; software, C.E.U.; validation, C.E.U. and J.-S.M.; formal analysis, Z.C., D.F.S. and C.E.U.; investigation, C.E.U.; resources D.F.S. and J.-S.M.; data curation Z.C., D.F.S., C.E.U. and J.-S.M.; writing—original draft preparation D.F.S., Z.C. and C.E.U.; writing—review and editing D.F.S., C.E.U. and J.-S.M.; visualization, C.E.U. and J.-S.M.; supervision, D.F.S. and J.-S.M.; project administration, D.F.S. and J.-S.M.; funding acquisition, D.F.S. and J.-S.M. All authors have read and agreed to the published version of the manuscript.

Funding: This research was funded by the National Science Foundation grant numbers CBET-2035302 and CBET-2035280 and The Joint Center for Deployment and Research in Earth Abundant Materials (JCDREAM) in Washington State.

Data Availability Statement: The original contributions presented in this study are included in the article/Supplementary Materials. Further inquiries can be directed to the corresponding authors.

Acknowledgments: The authors would like to thank Roger Moulton at SACHEM for the high trans content OSDA used in this work. The authors would also like to acknowledge National Science Foundation Awards CBET-2035302 and CBET-2035280 for financial support. This work was partially funded by the Joint Center for Deployment and Research in Earth Abundant Materials (JCDREAM) in Washington State. This work also used Bridges-2 at the Pittsburgh Supercomputer Center through allocation CHE170068 from the Advanced Cyberinfrastructure Coordination Ecosystem: Services & Support (ACCESS) program, which is supported by National Science Foundation grants #2138259, #2138286, #2138307, #2137603, and #213829641. Additional computational resources were provided by the Kamiak HPC under the Center for Institutional Research Computing at Washington State University. The Pacific Northwest National Laboratory is operated by Battelle for the U.S. DOE.

Conflicts of Interest: The authors declare no conflict of interest.

References

1. Burton, A.W.; Lee, G.S.; Zones, S.I. Phase Selectivity in the Syntheses of Cage-Based Zeolite Structures: An Investigation of Thermodynamic Interactions between Zeolite Hosts and Structure Directing Agents by Molecular Modeling. *Microporous Mesoporous Mater.* **2006**, *90*, 129–144. [CrossRef]
2. Cundy, C.S.; Cox, P.A. The Hydrothermal Synthesis of Zeolites: Precursors, Intermediates and Reaction Mechanism. *Microporous Mesoporous Mater.* **2005**, *82*, 1–78. [CrossRef]
3. Dusselier, M.; Davis, M.E. Small-Pore Zeolites: Synthesis and Catalysis. *Chem. Rev.* **2018**, *118*, 5265–5329. [CrossRef]
4. Li, J.; Corma, A.; Yu, J. Synthesis of New Zeolite Structures. *Chem. Soc. Rev.* **2015**, *44*, 7112–7127. [CrossRef]
5. Meng, X.; Xiao, F.-S. Green Routes for Synthesis of Zeolites. *Chem. Rev.* **2014**, *114*, 1521–1543. [CrossRef] [PubMed]
6. Schmidt, J.E.; Deem, M.W.; Davis, M.E. Synthesis of a Specified, Silica Molecular Sieve by Using Computationally Predicted Organic Structure-Directing Agents. *Angew. Chem. Int. Ed.* **2014**, *53*, 8372–8374. [CrossRef] [PubMed]
7. Di Iorio, J.R.; Gounder, R. Controlling the Isolation and Pairing of Aluminum in Chabazite Zeolites Using Mixtures of Organic and Inorganic Structure-Directing Agents. *Chem. Mater.* **2016**, *28*, 2236–2247. [CrossRef]
8. Li, S.; Li, J.; Dong, M.; Fan, S.; Zhao, T.; Wang, J.; Fan, W. Strategies to Control Zeolite Particle Morphology. *Chem. Soc. Rev.* **2019**, *48*, 885–907. [CrossRef]

9. Moliner, M.; Martínez, C.; Corma, A. Multipore Zeolites: Synthesis and Catalytic Applications. *Angew. Chem. Int. Ed.* **2015**, *54*, 3560–3579. [CrossRef]
10. Wagner, P.; Nakagawa, Y.; Lee, G.S.; Davis, M.E.; Elomari, S.; Medrud, R.C.; Zones, S.I. Guest/Host Relationships in the Synthesis of the Novel Cage-Based Zeolites SSZ-35, SSZ-36, and SSZ-39. *J. Am. Chem. Soc.* **2000**, *122*, 263–273. [CrossRef]
11. Zones, S.I.; Burton, A.W.; Lee, G.S.; Olmstead, M.M. A Study of Piperidinium Structure-Directing Agents in the Synthesis of Silica Molecular Sieves under Fluoride-Based Conditions. *J. Am. Chem. Soc.* **2007**, *129*, 9066–9079. [CrossRef]
12. Gábová, V.; Dědeček, J.; Čejka, J. Control of Al Distribution in ZSM-5 by Conditions of Zeolite Synthesis. *Chem. Commun.* **2003**, 1196–1197. [CrossRef] [PubMed]
13. Borry, R.W.; Kim, Y.H.; Huffsmith, A.; Reimer, J.A.; Iglesia, E. Structure and Density of Mo and Acid Sites in Mo-Exchanged H-ZSM5 Catalysts for Nonoxidative Methane Conversion. *J. Phys. Chem. B* **1999**, *103*, 5787–5796. [CrossRef]
14. Bortnovsky, O.; Sobalík, Z.; Wichterlová, B. Exchange of Co(II) Ions in H-BEA Zeolites: Identification of Aluminum Pairs in the Zeolite Framework. *Microporous Mesoporous Mater.* **2001**, *46*, 265–275. [CrossRef]
15. Dědeček, J.; Kaucký, D.; Wichterlová, B. Co^{2+} Ion Siting in Pentasil-Containing Zeolites, Part 3. *Microporous Mesoporous Mater.* **2000**, *35–36*, 483–494. [CrossRef]
16. Dědeček, J.; Kaucký, D.; Wichterlová, B. Al Distribution in ZSM-5 Zeolites: An Experimental Study. *Chem. Commun.* **2001**, 970–971. [CrossRef]
17. Dědeček, J.; Kaucký, D.; Wichterlová, B.; Gonsiorová, O. Co^{2+} Ions as Probes of Al Distribution in the Framework of Zeolites. ZSM-5 Study. *Phys. Chem. Chem. Phys.* **2002**, *4*, 5406–5413. [CrossRef]
18. Dědeček, J.; Wichterlová, B. Co^{2+} Ion Siting in Pentasil-Containing Zeolites. I. Co^{2+} Ion Sites and Their Occupation in Mordenite. A Vis−NIR Diffuse Reflectance Spectroscopy Study. *J. Phys. Chem. B* **1999**, *103*, 1462–1476. [CrossRef]
19. Bohinc, R.; Hoszowska, J.; Dousse, J.-C.; Błachucki, W.; Zeeshan, F.; Kayser, Y.; Nachtegaal, M.; Pinar, A.B.; van Bokhoven, J.A. Distribution of Aluminum over Different T-Sites in Ferrierite Zeolites Studied with Aluminum Valence to Core X-Ray Emission Spectroscopy. *Phys. Chem. Chem. Phys.* **2017**, *19*, 29271–29277. [CrossRef]
20. Chen, J.; Liang, T.; Li, J.; Wang, S.; Qin, Z.; Wang, P.; Huang, L.; Fan, W.; Wang, J. Regulation of Framework Aluminum Siting and Acid Distribution in H-MCM-22 by Boron Incorporation and Its Effect on the Catalytic Performance in Methanol to Hydrocarbons. *ACS Catal.* **2016**, *6*, 2299–2313. [CrossRef]
21. Dedecek, J.; Balgová, V.; Pashkova, V.; Klein, P.; Wichterlová, B. Synthesis of ZSM-5 Zeolites with Defined Distribution of Al Atoms in the Framework and Multinuclear MAS NMR Analysis of the Control of Al Distribution. *Chem. Mater.* **2012**, *24*, 3231–3239. [CrossRef]
22. Kim, C.W.; Heo, N.H.; Seff, K. Framework Sites Preferred by Aluminum in Zeolite ZSM-5. Structure of a Fully Dehydrated, Fully Cs^{+} -Exchanged ZSM-5 Crystal (MFI, Si/Al = 24). *J. Phys. Chem. C* **2011**, *115*, 24823–24838. [CrossRef]
23. Pashkova, V.; Klein, P.; Dedecek, J.; Tokarová, V.; Wichterlová, B. Incorporation of Al at ZSM-5 Hydrothermal Synthesis. Tuning of Al Pairs in the Framework. *Microporous Mesoporous Mater.* **2015**, *202*, 138–146. [CrossRef]
24. Pashkova, V.; Sklenak, S.; Klein, P.; Urbanova, M.; Dědeček, J. Location of Framework Al Atoms in the Channels of ZSM-5: Effect of the (Hydrothermal) Synthesis. *Chem.-Eur. J.* **2016**, *22*, 3937–3941. [CrossRef]
25. Pinar, A.B.; Gómez-Hortigüela, L.; McCusker, L.B.; Pérez-Pariente, J. Controlling the Aluminum Distribution in the Zeolite Ferrierite via the Organic Structure Directing Agent. *Chem. Mater.* **2013**, *25*, 3654–3661. [CrossRef]
26. Song, C.; Chu, Y.; Wang, M.; Shi, H.; Zhao, L.; Guo, X.; Yang, W.; Shen, J.; Xue, N.; Peng, L.; et al. Cooperativity of Adjacent Brønsted Acid Sites in MFI Zeolite Channel Leads to Enhanced Polarization and Cracking of Alkanes. *J. Catal.* **2017**, *349*, 163–174. [CrossRef]
27. Vjunov, A.; Fulton, J.L.; Huthwelker, T.; Pin, S.; Mei, D.; Schenter, G.K.; Govind, N.; Camaioni, D.M.; Hu, J.Z.; Lercher, J.A. Quantitatively Probing the Al Distribution in Zeolites. *J. Am. Chem. Soc.* **2014**, *136*, 8296–8306. [CrossRef]
28. Yokoi, T.; Mochizuki, H.; Biligetu, T.; Wang, Y.; Tatsumi, T. Unique Al Distribution in the MFI Framework and Its Impact on Catalytic Properties. *Chem. Lett.* **2017**, *46*, 798–800. [CrossRef]
29. Yokoi, T.; Mochizuki, H.; Namba, S.; Kondo, J.N.; Tatsumi, T. Control of the Al Distribution in the Framework of ZSM-5 Zeolite and Its Evaluation by Solid-State NMR Technique and Catalytic Properties. *J. Phys. Chem. C* **2015**, *119*, 15303–15315. [CrossRef]
30. Schmithorst, M.B.; Prasad, S.; Moini, A.; Chmelka, B.F. Direct Detection of Paired Aluminum Heteroatoms in Chabazite Zeolite Catalysts and Their Significance for Methanol Dehydration Reactivity. *J. Am. Chem. Soc.* **2023**, *145*, 18215–18220. [CrossRef]
31. Di Iorio, J.R.; Li, S.; Jones, C.B.; Nimlos, C.T.; Wang, Y.; Kunkes, E.; Vattipalli, V.; Prasad, S.; Moini, A.; Schneider, W.F.; et al. Cooperative and Competitive Occlusion of Organic and Inorganic Structure-Directing Agents within Chabazite Zeolites Influences Their Aluminum Arrangement. *J. Am. Chem. Soc.* **2020**, *142*, 4807–4819. [CrossRef]

32. Di Iorio, J.R.; Nimlos, C.T.; Gounder, R. Introducing Catalytic Diversity into Single-Site Chabazite Zeolites of Fixed Composition via Synthetic Control of Active Site Proximity. *ACS Catal.* **2017**, *7*, 6663–6674. [CrossRef]
33. Wang, X.; Wang, Y.; Moini, A.; Gounder, R.; Maginn, E.J.; Schneider, W.F. Influence of an *N*, *N*, *N*-Trimethyl-1-Adamantyl Ammonium ($TMAda^+$) Structure Directing Agent on Al Distributions and Pair Features in Chabazite Zeolite. *Chem. Mater.* **2022**, *34*, 10811–10822. [CrossRef]
34. Lee, S.; Nimlos, C.T.; Kipp, E.R.; Wang, Y.; Gao, X.; Schneider, W.F.; Lusardi, M.; Vattipalli, V.; Prasad, S.; Moini, A.; et al. Evolution of Framework Al Arrangements in CHA Zeolites during Crystallization in the Presence of Organic and Inorganic Structure-Directing Agents. *Cryst. Growth Des.* **2022**, *22*, 6275–6295. [CrossRef]
35. Krishna, S.H.; Goswami, A.; Wang, Y.; Jones, C.B.; Dean, D.P.; Miller, J.T.; Schneider, W.F.; Gounder, R. Influence of Framework Al Density in Chabazite Zeolites on Copper Ion Mobility and Reactivity during NO_x Selective Catalytic Reduction with NH_3. *Nat. Catal.* **2023**, *6*, 276–285. [CrossRef]
36. Theis, J.R.; Ura, J.; Getsoian, A.B.; Prikhodko, V.Y.; Thomas, C.R.; Pihl, J.A.; Lardinois, T.M.; Gounder, R.; Wei, X.; Ji, Y.; et al. Effect of Framework Al Pairing on NO Storage Properties of Pd-CHA Passive NO_x Adsorbers. *Appl. Catal. B* **2023**, *322*, 122074. [CrossRef]
37. Umhey, C.E.; Guo, J.; Cui, Z.; Shantz, D.F.; Kulkarni, A.; McEwen, J.-S. Elucidating the Impact of *Cis–Trans* Organic Structure Directing Agent Isomer Ratios on the Aluminum Distribution Within SSZ-39. *Chem. Mater.* **2024**, *36*, 11852–11862. [CrossRef]
38. Kakiuchi, Y.; Yamasaki, Y.; Tsunoji, N.; Takamitsu, Y.; Sadakane, M.; Sano, T. One-Pot Synthesis of Phosphorus-Modified AEI Zeolites Derived by the Dual-Template Method as a Durable Catalyst with Enhanced Thermal/Hydrothermal Stability for Selective Catalytic Reduction of NO_x by NH_3. *Chem. Lett.* **2016**, *45*, 122–124. [CrossRef]
39. Xu, H.; Zhu, L.; Wu, Q.; Meng, X.; Xiao, F.-S. Advances in the Synthesis and Application of the SSZ-39 Zeolite. *Inorg. Chem. Front.* **2022**, *9*, 1047–1057. [CrossRef]
40. Sada, Y.; Chokkalingam, A.; Iyoki, K.; Yoshioka, M.; Ishikawa, T.; Naraki, Y.; Yanaba, Y.; Yamada, H.; Ohara, K.; Sano, T.; et al. Tracking the Crystallization Behavior of High-Silica FAU during AEI-Type Zeolite Synthesis Using Acid Treated FAU-Type Zeolite. *RSC Adv.* **2021**, *11*, 23082–23089. [CrossRef]
41. Tsunoji, N.; Shimono, D.; Tsuchiya, K.; Sadakane, M.; Sano, T. Formation Pathway of AEI Zeolites as a Basis for a Streamlined Synthesis. *Chem. Mater.* **2020**, *32*, 60–74. [CrossRef]
42. Guo, A.; Liu, H.; Li, Y.; Luo, Y.; Ye, D.; Jiang, J.; Chen, P. Recent Progress in Novel Zeolite Catalysts for Selective Catalytic Reduction of Nitrogen Oxides. *Catal. Today* **2023**, *422*, 114212. [CrossRef]
43. Moliner, M.; Franch, C.; Palomares, E.; Grill, M.; Corma, A. Cu–SSZ-39, an Active and Hydrothermally Stable Catalyst for the Selective Catalytic Reduction of NO_x. *Chem. Commun.* **2012**, *48*, 8264. [CrossRef]
44. Dusselier, M.; Deimund, M.A.; Schmidt, J.E.; Davis, M.E. Methanol-to-Olefins Catalysis with Hydrothermally Treated Zeolite SSZ-39. *ACS Catal.* **2015**, *5*, 6078–6085. [CrossRef]
45. Wulfers, M.J.; Teketel, S.; Ipek, B.; Lobo, R.F. Conversion of Methane to Methanol on Copper-Containing Small-Pore Zeolites and Zeotypes. *Chem. Commun.* **2015**, *51*, 4447–4450. [CrossRef]
46. Ransom, R.; Coote, J.; Moulton, R.; Gao, F.; Shantz, D.F. Synthesis and Growth Kinetics of Zeolite SSZ-39. *Ind. Eng. Chem. Res.* **2017**, *56*, 4350–4356. [CrossRef]
47. Ransom, R.; Moulton, R.; Shantz, D.F. The Structure Directing Agent Isomer Used in SSZ-39 Synthesis Impacts the Zeolite Activity towards Selective Catalytic Reduction of Nitric Oxides. *J. Catal.* **2020**, *382*, 339–346. [CrossRef]
48. Pokhrel, J.; Shantz, D.F. Continuous Partial Oxidation of Methane to Methanol over Cu-SSZ-39 Catalysts. *J. Catal.* **2023**, *421*, 300–308. [CrossRef]
49. Dusselier, M.; Schmidt, J.E.; Moulton, R.; Haymore, B.; Hellums, M.; Davis, M.E. Influence of Organic Structure Directing Agent Isomer Distribution on the Synthesis of SSZ-39. *Chem. Mater.* **2015**, *27*, 2695–2702. [CrossRef]
50. Cui, Z.; Umhey, C.E.; Ukagha, O.C.; Ogunleye, M.; McEwen, J.-S.; Shantz, D.F. Quantifying How the *Cis*/*Trans* Ratio of *N*, *N*-Dimethyl-3,5-Dimethylpiperidinium Hydroxide Impacts the Growth Kinetics, Composition and Local Structure of SSZ-39. *RSC Adv.* **2025**, *15*, 7962–7972. [CrossRef] [PubMed]
51. Kresse, G.; Furthmüller, J. Efficient Iterative Schemes for Ab Initio Total-Energy Calculations Using a Plane-Wave Basis Set. *Phys. Rev. B* **1996**, *54*, 11169–11186. [CrossRef]
52. Kresse, G.; Furthmüller, J. Efficiency of Ab-Initio Total Energy Calculations for Metals and Semiconductors Using a Plane-Wave Basis Set. *Comput. Mater. Sci.* **1996**, *6*, 15–50. [CrossRef]
53. Kresse, G.; Hafner, J. Ab Initio Molecular Dynamics for Liquid Metals. *Phys. Rev. B* **1993**, *47*, 558–561. [CrossRef] [PubMed]
54. Kresse, G.; Joubert, D. From Ultrasoft Pseudopotentials to the Projector Augmented-Wave Method. *Phys. Rev. B* **1999**, *59*, 1758–1775. [CrossRef]

55. Lejaeghere, K.; Bihlmayer, G.; Björkman, T.; Blaha, P.; Blügel, S.; Blum, V.; Caliste, D.; Castelli, I.E.; Clark, S.J.; Dal Corso, A.; et al. Reproducibility in Density Functional Theory Calculations of Solids. *Science* **2016**, *351*, aad3000. [CrossRef] [PubMed]
56. Klimeš, J.; Bowler, D.R.; Michaelides, A. Van Der Waals Density Functionals Applied to Solids. *Phys. Rev. B* **2011**, *83*, 195131. [CrossRef]

Disclaimer/Publisher's Note: The statements, opinions and data contained in all publications are solely those of the individual author(s) and contributor(s) and not of MDPI and/or the editor(s). MDPI and/or the editor(s) disclaim responsibility for any injury to people or property resulting from any ideas, methods, instructions or products referred to in the content.